

---

# Accelerating spiking neural network training

---

**Luke Taylor**  
University of Oxford  
Oxford, United Kingdom  
luke.taylor@hertford.ox.ac.uk

**Andrew King**  
University of Oxford  
Oxford, United Kingdom  
andrew.king@dpag.ox.ac.uk

**Nicol Harper**  
University of Oxford  
Oxford, United Kingdom  
nicol.harper@dpag.ox.ac.uk

## Abstract

Spiking neural networks (SNN) are a type of artificial network inspired by the use of action potentials in the brain. There is a growing interest in emulating these networks on neuromorphic computers due to their improved energy consumption and speed, which are the main scaling issues of their counterpart the artificial neural network (ANN). Significant progress has been made in directly training SNNs to perform on par with ANNs in terms of accuracy. These methods are however slow due to their sequential nature, leading to long training times. We propose a new technique for directly training single-spike-per-neuron SNNs which eliminates all sequential computation and relies exclusively on vectorised operations. We demonstrate over a  $\times 10$  speedup in training with robust classification performance on real datasets of low to medium spatio-temporal complexity (Fashion-MNIST and Neuromorphic-MNIST). Our proposed solution manages to solve certain tasks with over a 95.68% reduction in spike counts relative to a conventionally trained SNN, which could significantly reduce energy requirements when deployed on neuromorphic computers.

## 1 Introduction

An aspiration of neuromorphic engineering is to design new computers that match the computational power and energy efficiency of the human brain. The human brain consists on the scale of  $10^{11}$  neurons [2] and consumes approximately 20 watts of power [44]. Current engineering efforts pail in comparison, with the largest artificial neural networks (ANNs) consisting of far less neural units and consuming magnitudes more energy [45]. Undeniably ANNs have achieved amazing feats over recent years by matching or surpassing human level performance in natural language processing problems [5], auditory and visual recognition tasks [13, 12] and challenging games [26, 43, 46]. However, as the problem difficulty increases, so has the size of the neural networks required to solve them. Most notably, the GPT language models have increased from 110 million to 1.5 billion to 175 billion parameters in order to deliver ever improving language comprehension [34, 35, 5]. Such scaling is not sustainable due to the substantial energy demands associated with these growing networks [45, 40].

Spiking neural networks (SNNs) are a particular type of neural network in which neurons communicate via spikes rather than graded potentials. These networks have theoretically been shown to match the performance of ANNs [25] and in particular practical cases can do so [53, 3], whilst greatly reducing the required energy consumption when deployed on neuromorphic hardware [50]. Although we are on a promising path towards constructing and scaling neuromorphic computers [9, 52], we

are yet to fully comprehend how to properly train SNNs [54]. To date, the most effective training methods are performed off-line on a GPU before porting learned synaptic weights to neuromorphic hardware [10]. One such training method is to use an ANN to learn the synaptic weights of a SNN. This can be achieved by mapping pre-trained ANNs to SNNs [36, 37], training ANNs with particular activation functions which emulate neuron dynamics [16, 24] or by coupling ANN and SNN training by using the SNN for the forward pass and the ANN for the backward pass [48, 49, 17]. Notably these methods disregard the temporal spiking nature and constrain SNNs to a rate-code, which 1) slows down inference due to the long simulation periods required to achieve reasonable prediction accuracies and 2) as a result do not necessarily improve the energy efficiency over ANNs [8]. Another approach to overcoming these shortcomings is to directly train a SNN and permit network computation to be performed through the timing of spikes. Backpropagation through time (BPTT) can be employed, as the SNN is a particular form of recurrent neural network [27]. However, BPTT requires the network of optimisation to be differentiable, which a SNN violates due to the non-differentiable spiking dynamics. This issue can be circumvented by either smoothing the spike function [14] or by replacing the gradient of the non-differentiable spike function with a surrogate derivative function [27, 42, 55].

To date, most research has focused on directly training SNNs in order to improve prediction accuracies, largely neglecting their slow training times. Some work has increased training speeds by reframing the backward pass by taking advantage of network spike sparsity [32] or by completely removing the backward pass and performing all learning in an online fashion [3]. Although these techniques are promising, one of the main bottlenecks to accelerating SNN training is the sequential nature of this process, which precludes efficient parallelisation on GPUs. We address this issue, for which our **main contributions** can be summarised as follows:

1. We propose a new algorithmic SNN training approach called FastSNN, which eliminates all slow sequential computation and exclusively relies on fast GPU parallelisable tensor operations.
2. We experimentally evaluate the speedup of our method, demonstrating drastic training acceleration over a variety of layer units and simulation steps, achieving over a  $\times 16.94$  training and  $\times 26.71$  inference speedup for shallow networks simulated over short timespans using modest batch sizes.
3. We explore the classification accuracy of our training method and demonstrate reasonable prediction performance on real datasets of low to medium spatiotemporal complexity (such as the Fashion-MNIST [51] and Neuromorphic-MNIST [28] datasets).
4. Due to the single-spike-per-neuron assumption, our method is theoretically able to achieve increased energy efficiency on neuromorphic hardware by reducing the number of network spikes by over 95.68% for certain problems.

To the best of our knowledge, we present here the fastest approach for directly training SNNs, which will hopefully contribute towards the goal of accelerating SNN training to solve more demanding real-world problems.

## 2 Accelerating spiking neural networks

### 2.1 Standard SNN model

A spiking neural network (SNN) is a network of neurons which communicate with each other using binary signals known as spikes (Figure 1a). For simplicity we focus on standard feedforward SNNs which consist of  $L$  fully connected layers, where each layer  $l$  consists of  $N^{(l)}$  spiking neurons that are fully connected to the next  $l + 1$  layer via synaptic weights  $W^{(l+1)} \in \mathbb{R}^{N^{(l+1)} \times N^{(l)}}$ . Every neuron  $i$  in layer  $l$  is characterised by a spike output  $S_i^{(l)}[t] = f(V_i^{(l)}[t]) \in \{0, 1\}$  ( $f$  is the spike function) and a membrane potential  $V_i^{(l)}[t] \in \mathbb{R}$ , which is raised or lowered by input current  $I_i^{(l)}[t] \in \mathbb{R}$  at every simulation step  $t \in \{1, \dots, T\}$  for  $T \in \mathbb{N}$ . Membrane potentials are evolved according to the leaky integrate and fire (LIF) model

$$\tau \frac{dV_i^{(l)}(t)}{dt} = -V_i^{(l)}(t) + V_{rest} + RI_i^{(l)}(t) \quad (1)$$

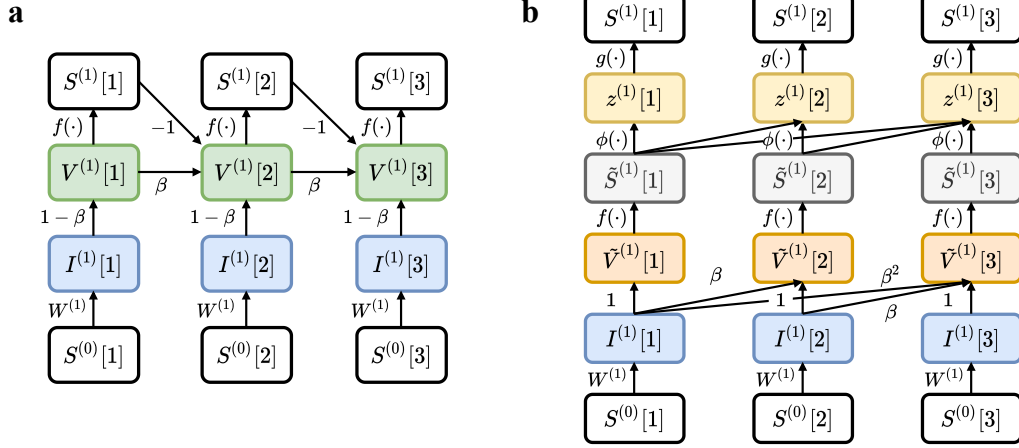


Figure 1: Schematics of the computational graphs of a single layer of the standard SNN and FastSNN. **a.** Standard SNN (modified from [27]): Input spikes  $S^{(0)}[t]$  induce currents  $I^{(1)}[t]$  through feedforward weights  $W^{(1)}$ , which charge membrane potentials  $V^{(1)}[t]$  resulting in output spikes  $S^{(1)}[t]$  if firing threshold is reached. Furthermore, the membrane potentials  $V^{(1)}[t]$  recurrently depend on membrane potentials  $V^{(1)}[t-1]$  and output spikes  $S^{(1)}[t-1]$  (for reset). **b.** FastSNN: Unlike in the standard SNN, we compute membrane potentials  $\tilde{V}^{(1)}[t]$  without reset and obtain a convolutional form. These no-reset membrane potentials  $\tilde{V}^{(1)}[t]$  are mapped to erroneous output spikes  $\tilde{S}^{(1)}[t]$ , which are consequentially mapped to an intermediate latent representation  $\tilde{z}^{(1)}[t]$  via proposed function  $\phi$  (proposition 1). Finally, correct output spikes  $S^{(1)}[t]$  are obtained by passing  $\tilde{z}^{(1)}[t]$  through proposed function  $g$  (proposition 2).

where  $V_{rest} \in \mathbb{R}$  is the resting potential,  $\tau \in \mathbb{R}$  is the membrane time constant and  $R \in \mathbb{R}$  is the input resistance [11]. Without loss of generality the LIF model is normalised ( $V_i^{(l)}(t) \in [0, 1]$  by  $V_{rest} = 0, V_{th} = 1, R = 1$ ; see supplementary) and discretised using the forward Euler method (see supplementary), from which the membrane potentials are updated using the following difference equation.

$$V_i^{(l)}[t+1] = \beta V_i^{(l)}[t] + \underbrace{(1-\beta) \left( b_i^{(l)} + \sum_{j=1}^{N^{(l-1)}} W_{ij}^{(l)} S_j^{(l-1)}[t+1] \right)}_{\text{Input current } I_i^{(l)}[t+1]} - \underbrace{S_i^{(l)}[t]}_{\text{Spike reset}} \quad (2)$$

The membrane potential is charged from the current induced by the incoming presynaptic spikes  $S^{(l-1)}[t] \in \mathbb{R}^{N^{(l-1)}}$  and from the constant bias current source  $b_i^{(l)}$ . Overtime this potential dissipates, where the degree of dissipation is captured by  $\beta = \exp(-\frac{\Delta t}{\tau})$  (for simulation time resolution  $\Delta t \in \mathbb{R}$ ). The neurons membrane potential is at resting state  $V_{rest} = 0$  in the absence of any input current and emits a spike  $S_i^{(l)}[t] = 1$  if the potential rises above firing threshold  $V_{th} = 1$  (after which it reduced back close to resting state).

$$f(V_i^{(l)}[t]) = \begin{cases} 1, & \text{if } V_i^{(l)}[t] > 1 \\ 0, & \text{otherwise} \end{cases} \quad (3)$$

Optimising network weights using standard gradient descent is not directly possible due to the non-differentiable spiking function  $f$ . However, replacing the undefined derivate of function  $f$  with a surrogate gradient [27] permits the use of backprop [38] to optimise network weights with respect to a provided differentiable loss function  $\mathcal{L}$ .

## 2.2 FastSNN: Accelerated SNN model

A major hinderance in realising the full potential of SNNs is their slow training speeds. SNN training is conventionally conducted on graphical processing units (GPUs) [27, 56, 33, 32], although an active area of research strives to permit training directly on neuromorphic hardware [9, 31, 18, 19] (or a combination thereof [39, 6]). Training on GPUs is slow as the network needs to be simulated for every time step (due to difference equation 2). This sequential nature prohibits effective parallelization, which has been pinnacle in the on-going deep learning revolution [22]. We outline a new algorithmic scheme for training SNNs on GPUs which eschews the sequential dependence, by restricting ourselves to neurons with feedforward connectivity that spike at most once (*i.e.* have an infinite refractory period).<sup>1</sup> Our model (referred to as FastSNN) is comprised of three main steps and uses non-sequential operations that are readably implementable in modern auto differentiation frameworks [1, 30, 4] (Figure 1b).

**1. Convert presynaptic spikes to input current** We map the time series of presynaptic spikes  $S_j^{(l-1)}$ <sup>2</sup> to a time series of input currents  $I_i^{(l)}$ , which is achieved using a tensor multiplication.

$$I_i^{(l)}[t] = \sum_{j=1}^{N^{(l-1)}} W_{ij}^{(l)} S_j^{(l-1)}[t] \quad (4)$$

**2. Calculate membrane potentials without reset** We calculate the time series of no-reset membrane potentials  $\tilde{V}_i^{(l)}$  from the input current  $I_i^{(l)}$ . Different to the standard model, we calculate membrane potentials without the reset mechanism by dropping the reset term  $-S_i^{(l)}[t]$  in Equation 2. By unrolling this modified equation (see supplementary), we obtain a convolutional form allowing us to calculate the no-reset membrane potentials  $\tilde{V}_i^{(l)}$  without any sequential operations.

$$\tilde{V}_i^{(l)}[t] = \beta^t V_i^{(l)}[0] + (1 - \beta) \sum_{k=1}^t \beta^{t-k} I_i^{(l)}[k] \quad (5)$$

**3. Map no-reset membrane potentials to output spikes** We now map the time series of no-reset membrane potentials  $\tilde{V}_i^{(l)}$  to output spikes  $S_i^{(l)}$ . We obtain a time series of erroneous output spikes  $\tilde{S}_i^{(l)}$  by passing no-reset membrane potentials  $\tilde{V}_i^{(l)}$  through the spike function  $f$  (equation 3).

$$\tilde{S}_i^{(l)}[t] = f(\tilde{V}_i^{(l)}[t]) \quad (6)$$

Due to the removal of the spike reset mechanism, only the first spike per neuron in  $\tilde{S}_i^{(l)}$  follows the dynamics set out by the LIF model (equation 2). Thus we need to remove all spikes succeeding the first spike occurrence (hence the single spike per neuron assumption) to comply with the correct LIF spiking dynamics. We achieve this by constructing correct output spikes  $S_i^{(l)}$  with  $S_i^{(l)}[t] = 0$  for  $t \in \{1, 2, \dots, T\}$  and  $S_i^{(l)}[t] = 1$  for smallest  $t$  satisfying  $\tilde{V}_i^{(l)}[t] > 1$  (if such  $\tilde{V}_i^{(l)}[t]$  exists).

A straightforward solution would be to iterate over all elements in  $\tilde{S}_i^{(l)}$  and set all spikes succeeding the first to zero, but such sequential calculation is the very problem we set out to remediate. We propose a vectorised solution to this problem which is comprised of two steps:

1. Create an intermediate tensor  $z_i^{(l)}$ , which sets all values besides the first spike occurrence to a value other than one,  $z_i^{(l)}[t] \neq 1$  for all  $t$  except smallest  $t$  satisfying  $\tilde{S}_i^{(l)}[t] = 1$  (if such

<sup>1</sup>The single spike assumption can be related to the LIF model through the inclusion of an adaptive firing threshold, which has been explored in prior work [3, 53] and has support in neuromorphic hardware [41, 47]. However, the FastSNN model employs the most extreme firing threshold adaptation, by setting neuron firing threshold to infinity after spiking.

<sup>2</sup>Bold face variables denote time series as arrays as opposed to time-dependent scalar values.

$t$  exists). This is achieved by passing  $\tilde{\mathbf{S}}_i^{(l)}$  through function  $\phi$  proposed in proposition 1,  $\mathbf{z}_i^{(l)} = \phi(\tilde{\mathbf{S}}_i^{(l)})$ .

2. Obtain correct output spikes  $\mathbf{S}_i^{(l)}$  by mapping every value in the intermediate tensor  $\mathbf{z}_i^{(l)}$  besides the value one to zero, which is achieved by passing  $\mathbf{z}_i^{(l)}$  through function  $g$  proposed in proposition 2,  $\mathbf{S}_i^{(l)} = g(\mathbf{z}_i^{(l)})$ .

**Proposition 1.** *Function  $\phi(\tilde{\mathbf{S}}_i^{(l)})[t] = \sum_{k=1}^t \sum_{m=1}^k \tilde{S}_i^{(l)}[m]$  acting on  $\tilde{\mathbf{S}}_i^{(l)} \in \{0, 1\}^T$  contains at most one element equal to one  $\phi(\tilde{\mathbf{S}}_i^{(l)})[t] = 1$  for smallest  $t$  satisfying  $\tilde{S}_i^{(l)}[t] = 1$  (if such  $t$  exists).*

*Proof.* We start our proof by expressing  $\phi(\tilde{\mathbf{S}}_i^{(l)})[t] = \sum_{m=1}^t \tilde{S}_i^{(l)}[m](t - m + 1)$  through following algebraic rearrangement.

$$\begin{aligned} \phi(\tilde{\mathbf{S}}_i^{(l)})[t] &= \sum_{k=1}^t \sum_{m=1}^k \tilde{S}_i^{(l)}[m] = \sum_{m=1}^t \sum_{k=m}^t \tilde{S}_i^{(l)}[m] \quad (\text{reversing the order of summation})^3 \\ &= \sum_{m=1}^t \tilde{S}_i^{(l)}[m] \sum_{k=m}^t 1 = \sum_{m=1}^t \tilde{S}_i^{(l)}[m](t - m + 1) \end{aligned} \quad (7)$$

Next, we proceed to show that  $\phi(\tilde{\mathbf{S}}_i^{(l)})$  contains at most one element equal to one  $\phi(\tilde{\mathbf{S}}_i^{(l)})[t] = 1$  for the smallest  $t$  satisfying  $\tilde{S}_i^{(l)}[t] = 1$  (if such  $t$  exists). Firstly,  $\phi(\tilde{\mathbf{S}}_i^{(l)})[t] = 0$  for  $t \in [1, T]$  if  $\tilde{S}_i^{(l)}[t] = 0$  for  $t \in [1, T]$  (by substitution into equation 7). Next, if  $\tilde{S}_i^{(l)}[t_1] = 1$  for smallest  $t_1 \in [1, T]$  then  $\phi(\tilde{\mathbf{S}}_i^{(l)})[t_1] = 1$  (by substitution into equation 7). There can exist no  $t_2 > t_1$  such that  $\phi(\tilde{\mathbf{S}}_i^{(l)})[t_2] = 1$  because from equation 7 it follows that

$$\begin{aligned} \phi(\tilde{\mathbf{S}}_i^{(l)})[t+1] &= \sum_{m=1}^{t+1} \tilde{S}_i^{(l)}[m]((t+1) - m + 1) \\ &= \sum_{m=1}^t \tilde{S}_i^{(l)}[m]((t+1) - m + 1) + \tilde{S}_i^{(l)}[t+1] \\ &= \sum_{m=1}^t \tilde{S}_i^{(l)}[m](t - m + 1) + \sum_{m=1}^t \tilde{S}_i^{(l)}[m] + \tilde{S}_i^{(l)}[t+1] \\ &= \phi(\tilde{\mathbf{S}}_i^{(l)})[t] + \sum_{m=1}^{t+1} \tilde{S}_i^{(l)}[m] \end{aligned} \quad (8)$$

Thus  $\phi(\tilde{\mathbf{S}}_i^{(l)})[t_2] > \phi(\tilde{\mathbf{S}}_i^{(l)})[t_1]$  for all  $t_2 > t_1$  as  $\sum_{m=1}^{t_2} \tilde{S}_i^{(l)}[m] \geq \sum_{m=1}^{t_1} \tilde{S}_i^{(l)}[m] = 1 > 0$ .  $\square$

**Proposition 2.** *Function  $g(t) = \text{ReLU}(t(1 - t) + 1)t$  maps  $g(1) = 1$  and  $g(t) = 0$  for  $t \in \{0, 2, 3, \dots\}$ .*

*Proof.*  $g(0) = 0$  and  $g(1) = 1$  follow from substitution and  $t(1 - t) + 1 < 0$  for  $t \geq 2$  leading to  $\text{ReLU}(t(1 - t) + 1) = 0$  and hence  $g(t) = 0$  for all  $t \geq 2$ .  $\square$

### 3 Experiments and results

We evaluate the speedup advantages, classification accuracy and spike sparsity of the FastSNN in comparison to the standard SNN model. All models were implemented using PyTorch [30] with benchmarks and training conducted on a cluster of NVIDIA Tesla V100 GPUs.

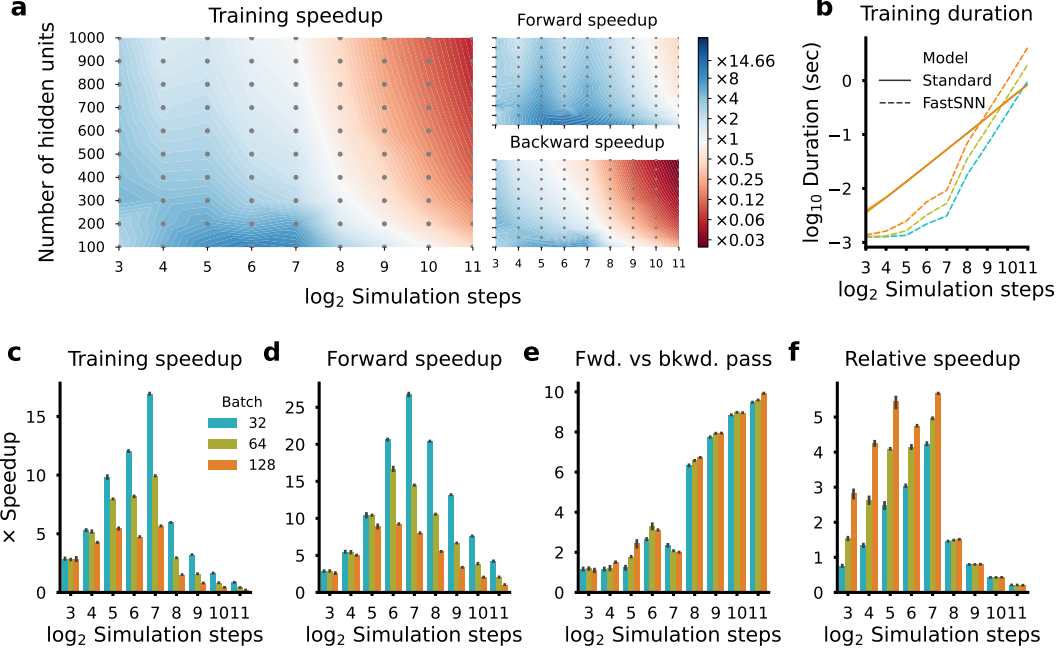


Figure 2: Speedup of the FastSNN over the standard SNN model for a single layer. **a.** Speedups as a function of the number of layer units and number of simulation steps for the total training step and the individual forward and backward passes (using a batch size  $b = 128$ ). **b.** Training durations for both models. Figures **b-f** use a layer with  $n = 200$  units and are a 10 sample average for which the mean and s.d. is plotted. **c.** Total training speedup of the FastSNN model. **d.** Forward pass speedup of the FastSN model. **e.** Forward vs the backward pass speedup of the FastSNN model. **f.** Relative speedup of the FastSNN using different batch sizes relative to the standard SNN using a fixed batch size  $b = 128$ .

### 3.1 Speedup benchmarks

We evaluate the speedup advantages of the FastSNN over the standard SNN model, by simulating the forward and backward passes of a single layer for a varying number of units and simulation steps. To do this, we generated a random input spike dataset (see supplementary) with a fixed number of input units ( $n = 10^3$ ) for a varying number of stimulation steps  $T$  (ranging from  $2^3$  to  $2^{11}$  in power of 2 increments). Every such dataset was passed through both SNN implementations for different numbers of units  $n$  (ranging from  $10^2$  to  $10^3$  in 100 unit increments) and batch sizes ( $b \in [32, 64, 128]$ ) and repeated 10 times (to account for trial-to-trial variability). Unless otherwise mentioned, the discussed results use a batch size of  $b = 128$  (commonly used for training) and  $n = 200$  units (comparable to what has often been used in prior SNN investigations [32, 56, 6, 33]).

#### 3.1.1 Robust speedup for different number of layer units and simulation steps

We observe a considerable training speedup across a range of different numbers of layer units and simulation steps (Figure 2a). We measure the training speedup as the ratio  $t_{\text{tot}}^{\text{SNN}} / t_{\text{tot}}^{\text{FastSNN}}$  where  $t_{\text{tot}}^{\text{SNN}} = t_{\text{fwd}}^{\text{SNN}} + t_{\text{bkw}}^{\text{SNN}}$  and  $t_{\text{tot}}^{\text{FastSNN}} = t_{\text{fwd}}^{\text{FastSNN}} + t_{\text{bkw}}^{\text{FastSNN}}$  are the total durations it takes the SNN and FastSNN to complete a forward and backward pass for a batch of data ( $b = 128$ ) respectively. These total speedups are most noticeable for a smaller number of units and simulation steps, with peak speedup of  $\times 9.32$  obtained for  $n = 100$  units and  $T = 2^6$  stimulation steps. Furthermore, these speedups are more pronounced for smaller batch sizes and when benchmarking on more powerful GPU architectures such as the Tesla A100 (see supplementary). If we fix the number of units to

<sup>3</sup>Reversing the order of summation identity  $\sum_{k=1}^t \sum_{m=1}^k s_{km} = \sum_{m=1}^t \sum_{k=m}^t s_{km}$  for matrix  $s \in \mathbb{R}^{t \times t}$ . For vector  $s \in \mathbb{R}^t$  we obtain identity  $\sum_{k=1}^t \sum_{m=1}^k s_m = \sum_{m=1}^t \sum_{k=m}^t s_m$  by setting  $s_{km} = s_m$  for all  $1 \leq k \leq t$ .

$n = 200$ , we observe a  $\times 16.94$  speedup for batch size  $b = 32$  as opposed to a  $\times 5.67$  speedup for batch size  $b = 128$  when simulating for  $T = 2^7$  steps (Figure 2c).

### 3.1.2 Considerable speedup for inference

The most notable speedup obtained by the FastSNN model is in the forward pass, outperforming the standard SNN for nearly all tried combinations of unit numbers and simulation steps and obtaining a maximal speedup of  $\times 14.6$  for  $n = 100$  units and  $T = 2^7$  stimulation steps (Figure 2a). Again, if we fix the number of units to  $n = 200$ , we observe a more drastic speedup for smaller batch sizes, with batch size  $b = 32$  achieving over a  $\times 26.71$  speedup as opposed to the  $\times 8.01$  speedup for batch size  $b = 128$  when simulating for  $T = 2^7$  simulation steps (Figure 2d). Total training times start to rapidly increase for large number of simulation steps (Figure 2b), however this is due to the backward pass slowing down relative to the forward pass (as measured by  $t_{\text{bkw}}^{\text{FastSNN}} / t_{\text{fwd}}^{\text{FastSNN}}$ ; Figure 2e). The FastSNN still obtains a speedup for longer simulation steps (Figure 2c), making it an applicable model for fast inference of single-spike-per-neuron SNNs on GPUs.

### 3.1.3 Applicability to training on smaller GPUs

To date, most effective training of different neural networks has been achieved using relatively small batch sizes ( $b = 32$  to  $b = 256$ ) compared to the size of the training datasets. Larger batches would decrease training times, but lead to a loss in generalization performance [23]. Training a SNN using the standard or FastSNN approach permits standard batch sizes (*e.g.*  $b = 128$ ) on modern GPUs (*e.g.* Tesla V100 and A100 GPUs). This is however not necessarily the case on older GPUs (*e.g.* NVIDIA GeForce GTX 1060), where training only allows for smaller batch sizes due to the large memory demands of SNN training [32]. This raises the question as to whether there is still any noteworthy speedup when training a FastSNN using multiple smaller batches relative to training a standard SNN using larger batches? We investigate this question using the following metric.

$$\text{relative speedup} = \frac{T_{\text{tot}; b=B}^{\text{SNN}}}{n T_{\text{tot}; b=B/n}^{\text{FastSNN}}} \quad (9)$$

This measures the ratio between the time  $T_{\text{tot}; b=B}^{\text{SNN}}$  it takes to train a batch of size  $B = 128$  using the standard SNN relative to the time  $n T_{\text{tot}; b=B/n}^{\text{FastSNN}}$  it takes to train  $n$  batches of size  $b = 128/n$  using the FastSNN.<sup>4</sup> Fixing the number of units to  $n = 200$ , we observe over a  $\times 4$  speedup when training the FastSNN for  $T = 2^7$  simulation steps on batches of size  $b = 32$  relative to training the standard SNN on batches of size  $b = 128$  (Figure 2f).

## 3.2 Classification accuracy

We investigated the ability of the FastSNN to classify real data of increasing difficulty. As suggested by [32], these include the following datasets of increasing spatio-temporal complexity, which cover the most relevant applications of neuromorphic hardware. The simplest dataset is the Fashion-MNIST (F-MNIST) image dataset, where the aim is to classify different fashion items [51]. Here we convert each pixel value into at most one spike (see supplementary), resulting in a sparse code of low spatio-temporal complexity. Slightly more challenging is the Neuromorphic-MNIST (N-MNIST) dataset [28], where the aim is to classify spike representation of handwritten digits. Here, the MNIST dataset [21] is mapped into a spike code using a neuromorphic vision sensor, yielding a code of lower sparsity and higher spatio-temporal complexity (as it includes noise from the recording device and input neurons can spike multiple times). Lastly, we adopted the Spiking Heidelberg Dataset (SHD) [7], in which the aim is to classify audio representations of different spoken digits (in both English and German). Here, waveforms of spoken digits are converted into spikes using a model of auditory cells in the cochlear nucleus, resulting in the least sparse code with highest spatio-temporal complexity in comparison to the F-MNIST and N-MNIST datasets.<sup>5</sup>

<sup>4</sup>This metric is a proxy as we do not consider the time it takes to load data onto GPU, which we assume to be negligible compared to SNN training times with modern data loading pipelines [20].

<sup>5</sup>The F-MNIST dataset is released under the MIT License and the N-MNIST and SHD datasets are released under the Creative Commons Attribution 4.0 International License.

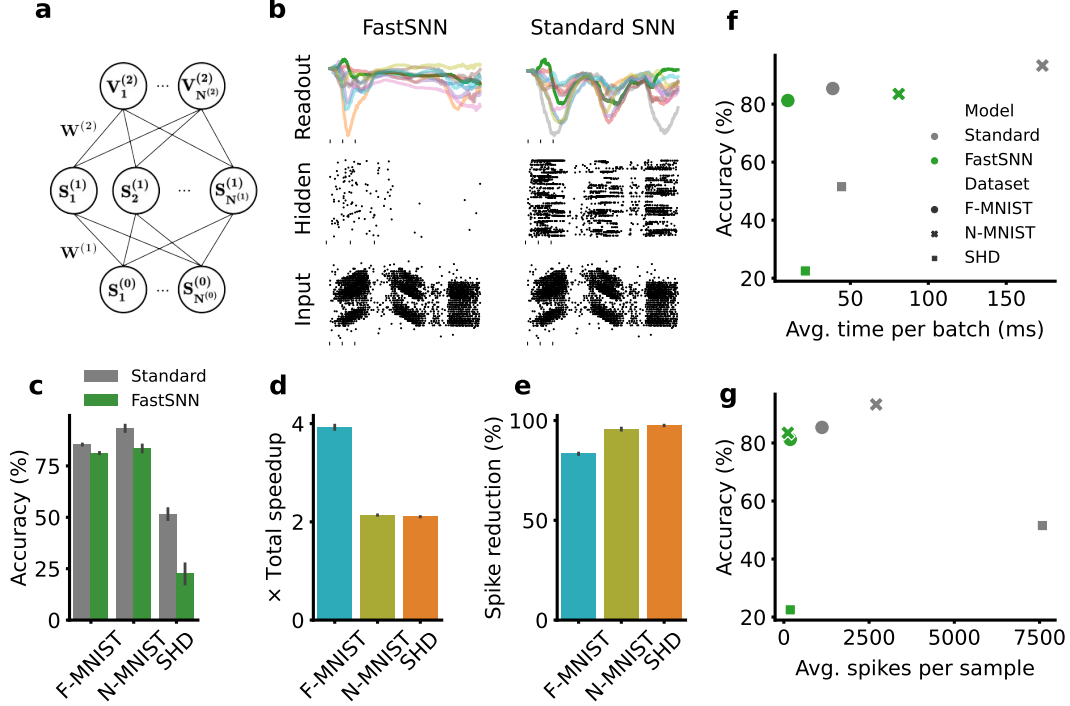


Figure 3: The classification performance and speedup of training the FastSNN on real datasets. **a.** Illustration of the network architecture used for training. **b.** Snapshot of the network activity after training of the FastSNN and standard SNN model in response to a sample from the N-MNIST dataset. Bottom: Spike raster of input sample. Middle: Spike raster of hidden unit activity. Top: Membrane potentials of the readout units (dark green line is the readout unit corresponding to the correct class). **c.** Classification accuracies of the FastSNN and standard SNN for the different datasets. Bar plots **c-e** represent a 6 sample mean with s.d.. **d.** Total training speedup of the FastSNN compared to the standard SNN for the different datasets. **e.** Spike count reduction of the FastSNN compared to the standard SNN on the different datasets. **f.** Model performance vs the average processing time of a training batch ( $b = 128$ ). **g.** Model performance vs the average number of spikes elicited per sample.

For all experiments we trained a two-layer fully connected network (Figure 3a) (using batches of size  $b = 128$ ), consisting of a hidden layer with  $n = 200$  units and a readout layer with a number of units corresponding to the size of the dataset trained on. As done in prior investigations [6, 7, 32, 33, 56], we set the readout units to have an infinite firing threshold and took predictions from those units that achieved maximum membrane potential over time. See supplementary for all training details.

### 3.2.1 Solving problems with low to medium spatio-temporal complexity

The FastSNN learns and generalises on datasets of low to medium spatio-temporal complexity, achieving a prediction accuracy of 81.23% and 83.50% on the F-MNIST and N-MNIST test datasets respectively, which are slightly less than the accuracies obtained by the standard SNN (F-MNIST 85.37%; N-MNIST 93.28%) (Figure 3c). Both models fare poorly on the SHD test dataset, with the FastSNN and standard SNN obtaining a 22.49% and 51.53% prediction accuracy respectively.

### 3.2.2 Drastic speedup in training

The FastSNN has an increased training speedup across all the datasets, obtaining a  $\times 3.92$ ,  $\times 2.13$  and  $\times 2.10$  for the F-MNIST, N-MNIST and SHD datasets respectively (Figure 3d). Differences in speedups across datasets are due to the different temporal lengths and input dimensions of the datasets. Apart from the SHD dataset, the FastSNN can be trained much faster than the standard SNN, for a slight reduction in performance accuracy (Figure 3f).



### 3.2.3 Extreme spike sparsity for the FastSNN

We inspected the number of spikes the FastSNN and standard SNN emit for each dataset. The interest in emulating SNNs on neuromorphic hardware is for their low energy consumption, which is approximately proportional to the number of spikes the network elicits [29, 53]. Due to the single-spike-per-neuron assumption of the FastSNN model, we observe extreme spike sparsity across the different datasets, with a 83.32%, 95.68% and 97.51% reduction in spike counts compared to the standard SNN model for the F-MNIST, N-MNIST and SHD datasets respectively (Figure 3e). This sparsity becomes visually apparent when viewing the spike raster of the hidden units of the FastSNN compared to the standard SNN on the N-MNIST dataset (Figure 3b). Notably, the FastSNN has only a slightly worse accuracy than the standard SNN on the F-MNIST and N-MNIST datasets despite providing a substantial reduction in spike counts (Figure 3g).

## 4 Discussion

Spiking neural networks (SNNs) emulated on neuromorphic hardware are an exciting avenue towards building computers which match the computational power and energy efficiency of the human brain. To date, most research efforts have focused on improving SNN prediction accuracies, with the downside that directly training SNNs is slow [32]. Our work aligns with the Green AI view [40], where instead of improving prediction accuracies, we instead focus on lowering computational cost through accelerated model training. We introduce a new training approach called FastSNN, which accelerates training of SNNs in which individual neurons can spike at most once. Our method eschews all sequential operations and solely relies on vectorised transformations, obtaining drastic training and inference speedups over conventional SNNs. These speedups are robust for different numbers of layer units and simulation steps, and even obtain noteworthy speedups when training using multiple smaller batches compared to training a standard SNN using larger batches, theoretically making training on older memory constrained GPUs viable. Furthermore, our method is able to obtain accelerated training and reasonable classification performance on real datasets of low to medium spatiotemporal complexity (F-MNIST:  $\times 3.92$  speedup and 81.23% accuracy; N-MNIST  $\times 2.13$  speedup and 83.50% accuracy). Lastly, due to the single-spike-per-neuron assumption, the FastSNN is able to predict the F-MNIST and N-MNIST datasets with a significant reduction in spike counts compared to the standard SNN (F-MNIST: 83.32% and N-MNIST: 95.68% spike reduction), which could further improve upon the energy requirements when deploying SNNs on neuromorphic hardware [29, 53].

**Limitations and future work** A scaling constraint of the FastSNN model is the backward pass, which drastically slows down for larger unit numbers and simulation lengths. A solution to overcoming this problem would be through the inclusion of sparse spiking gradient descent [32], which has been shown to accelerate the backward pass up to  $\times 150$  fold over the backward pass of standard SNN training. Furthermore, the FastSNN fails to obtain reasonable prediction accuracies on datasets of high spatio-temporal complexity, such as the SHD dataset. We find the single-spike-per-neuron assumption to impede network performance, as the standard SNN is able to obtain a 29% improvement in prediction accuracy likely due to the increase in spike activity. The standard feedforward SNN still fares poorly relative to other SNN investigations, due to the omission of recurrent connections and learnable membrane time constants, which have both been shown to obtain more generalisable performance on the SHD dataset [56, 53, 33]. Thus, it is reasonable to assume that such inclusions would also benefit the FastSNN model in obtaining increased prediction performance, which future investigations could explore.

## Acknowledgments and Disclosure of Funding

We thank Rob Pratt for helpful discussions. Luke Taylor was supported by the Clarendon Fund. Andrew King and Nicol Harper were supported by the Wellcome Trust (WT108369/Z/2015/Z).

## References

- [1] Martín Abadi, Paul Barham, Jianmin Chen, Zhifeng Chen, Andy Davis, Jeffrey Dean, Matthieu Devin, Sanjay Ghemawat, Geoffrey Irving, Michael Isard, et al. {TensorFlow}: A system for

- {Large-Scale} machine learning. In *12th USENIX symposium on operating systems design and implementation (OSDI 16)*, pages 265–283, 2016.
- [2] Frederico AC Azevedo, Ludmila RB Carvalho, Lea T Grinberg, José Marcelo Farfel, Renata EL Ferretti, Renata EP Leite, Wilson Jacob Filho, Roberto Lent, and Suzana Herculano-Houzel. Equal numbers of neuronal and nonneuronal cells make the human brain an isometrically scaled-up primate brain. *Journal of Comparative Neurology*, 513(5):532–541, 2009.
  - [3] Guillaume Bellec, Franz Scherr, Anand Subramoney, Elias Hajek, Darjan Salaj, Robert Legenstein, and Wolfgang Maass. A solution to the learning dilemma for recurrent networks of spiking neurons. *Nature communications*, 11(1):1–15, 2020.
  - [4] James Bradbury, Roy Frostig, Peter Hawkins, Matthew James Johnson, Chris Leary, Dougal Maclaurin, George Necula, Adam Paszke, Jake VanderPlas, Skye Wanderman-Milne, and Qiao Zhang. JAX: composable transformations of Python+NumPy programs, 2018.
  - [5] Tom B Brown, Benjamin Mann, Nick Ryder, Melanie Subbiah, Jared Kaplan, Prafulla Dhariwal, Arvind Neelakantan, Pranav Shyam, Girish Sastry, Amanda Askell, et al. Language models are few-shot learners. *arXiv preprint arXiv:2005.14165*, 2020.
  - [6] Benjamin Cramer, Sebastian Billaudelle, Simeon Kanya, Aron Leibfried, Andreas Grübl, Vitali Karasenko, Christian Pehle, Korbinian Schreiber, Yannik Stradmann, Johannes Weis, et al. Surrogate gradients for analog neuromorphic computing. *Proceedings of the National Academy of Sciences*, 119(4), 2022.
  - [7] Benjamin Cramer, Yannik Stradmann, Johannes Schemmel, and Friedemann Zenke. The heidelberg spiking data sets for the systematic evaluation of spiking neural networks. *IEEE Transactions on Neural Networks and Learning Systems*, 2020.
  - [8] Simon Davidson and Steve B Furber. Comparison of artificial and spiking neural networks on digital hardware. *Frontiers in Neuroscience*, 15:345, 2021.
  - [9] Mike Davies, Narayan Srinivasa, Tsung-Han Lin, Gautham Chinya, Yongqiang Cao, Sri Harsha Choday, Georgios Dimou, Prasad Joshi, Nabil Imam, Shweta Jain, et al. Loihi: A neuromorphic manycore processor with on-chip learning. *Ieee Micro*, 38(1):82–99, 2018.
  - [10] Steven K Esser, Paul A Merolla, John V Arthur, Andrew S Cassidy, Rathinakumar Appuswamy, Alexander Andreopoulos, David J Berg, Jeffrey L McKinstry, Timothy Melano, Davis R Barch, et al. Convolutional networks for fast, energy-efficient neuromorphic computing. *Proceedings of the national academy of sciences*, 113(41):11441–11446, 2016.
  - [11] Wulfram Gerstner, Werner M Kistler, Richard Naud, and Liam Paninski. *Neuronal dynamics: From single neurons to networks and models of cognition*. Cambridge University Press, 2014.
  - [12] Kaiming He, Xiangyu Zhang, Shaoqing Ren, and Jian Sun. Deep residual learning for image recognition. In *Proceedings of the IEEE conference on computer vision and pattern recognition*, pages 770–778, 2016.
  - [13] Geoffrey Hinton, Li Deng, Dong Yu, George E Dahl, Abdel-rahman Mohamed, Navdeep Jaitly, Andrew Senior, Vincent Vanhoucke, Patrick Nguyen, Tara N Sainath, et al. Deep neural networks for acoustic modeling in speech recognition: The shared views of four research groups. *IEEE Signal processing magazine*, 29(6):82–97, 2012.
  - [14] Dongsung Huh and Terrence J Sejnowski. Gradient descent for spiking neural networks. *arXiv preprint arXiv:1706.04698*, 2017.
  - [15] Eric Hunsberger. Spiking deep neural networks: Engineered and biological approaches to object recognition. 2018.
  - [16] Eric Hunsberger and Chris Eliasmith. Spiking deep networks with lif neurons. *arXiv preprint arXiv:1510.08829*, 2015.
  - [17] Saeed Reza Kheradpisheh, Maryam Mirsadeghi, and Timothée Masquelier. Spiking neural networks trained via proxy. *arXiv preprint arXiv:2109.13208*, 2021.
  - [18] Chul-Heung Kim, Soochang Lee, Sung Yun Woo, Won-Mook Kang, Suhwan Lim, Jong-Ho Bae, Jaeha Kim, and Jong-Ho Lee. Demonstration of unsupervised learning with spike-timing-dependent plasticity using a tft-type nor flash memory array. *IEEE Transactions on Electron Devices*, 65(5):1774–1780, 2018.

- [19] Dongseok Kwon, Suhwan Lim, Jong-Ho Bae, Sung-Tae Lee, Hyeongsu Kim, Young-Tak Seo, Seongbin Oh, Jangsaeng Kim, Kyuho Yeom, Byung-Gook Park, et al. On-chip training spiking neural networks using approximated backpropagation with analog synaptic devices. *Frontiers in neuroscience*, 14:423, 2020.
- [20] Guillaume Leclerc, Andrew Ilyas, Logan Engstrom, Sung Min Park, Hadi Salman, and Aleksander Madry. ffcv. <https://github.com/libffcv/ffcv/>, 2022. commit xxxxxxxx.
- [21] Yann LeCun. The mnist database of handwritten digits. <http://yann.lecun.com/exdb/mnist/>, 1998.
- [22] Yann LeCun, Yoshua Bengio, and Geoffrey Hinton. Deep learning. *nature*, 521(7553):436–444, 2015.
- [23] Yann A LeCun, Léon Bottou, Genevieve B Orr, and Klaus-Robert Müller. Efficient backprop. In *Neural networks: Tricks of the trade*, pages 9–48. Springer, 2012.
- [24] Qian Liu, Yunhua Chen, and Steve Furber. Noisy softplus: an activation function that enables snns to be trained as anns. *arXiv preprint arXiv:1706.03609*, 2017.
- [25] Wolfgang Maass. Networks of spiking neurons: the third generation of neural network models. *Neural networks*, 10(9):1659–1671, 1997.
- [26] Volodymyr Mnih, Koray Kavukcuoglu, David Silver, Andrei A Rusu, Joel Veness, Marc G Bellemare, Alex Graves, Martin Riedmiller, Andreas K Fidjeland, Georg Ostrovski, et al. Human-level control through deep reinforcement learning. *nature*, 518(7540):529–533, 2015.
- [27] Emre O Neftci, Hesham Mostafa, and Friedemann Zenke. Surrogate gradient learning in spiking neural networks: Bringing the power of gradient-based optimization to spiking neural networks. *IEEE Signal Processing Magazine*, 36(6):51–63, 2019.
- [28] Garrick Orchard, Ajinkya Jayawant, Gregory K Cohen, and Nitish Thakor. Converting static image datasets to spiking neuromorphic datasets using saccades. *Frontiers in neuroscience*, 9:437, 2015.
- [29] Priyadarshini Panda, Sai Aparna Aketi, and Kaushik Roy. Toward scalable, efficient, and accurate deep spiking neural networks with backward residual connections, stochastic softmax, and hybridization. *Frontiers in Neuroscience*, 14:653, 2020.
- [30] Adam Paszke, Sam Gross, Soumith Chintala, Gregory Chanan, Edward Yang, Zachary DeVito, Zeming Lin, Alban Desmaison, Luca Antiga, and Adam Lerer. Automatic differentiation in pytorch. 2017.
- [31] G Pedretti, V Milo, S Ambrogio, R Carboni, S Bianchi, A Calderoni, N Ramaswamy, AS Spinelli, and D Ielmini. Memristive neural network for on-line learning and tracking with brain-inspired spike timing dependent plasticity. *Scientific reports*, 7(1):1–10, 2017.
- [32] Nicolas Perez-Nieves and Dan FM Goodman. Sparse spiking gradient descent. *arXiv preprint arXiv:2105.08810*, 2021.
- [33] Nicolas Perez-Nieves, Vincent CH Leung, Pier Luigi Dragotti, and Dan FM Goodman. Neural heterogeneity promotes robust learning. *Nature communications*, 12(1):1–9, 2021.
- [34] Alec Radford, Karthik Narasimhan, Tim Salimans, and Ilya Sutskever. Improving language understanding by generative pre-training. 2018.
- [35] Alec Radford, Jeffrey Wu, Rewon Child, David Luan, Dario Amodei, Ilya Sutskever, et al. Language models are unsupervised multitask learners. *OpenAI blog*, 1(8):9, 2019.
- [36] Bodo Rueckauer, Iulia-Alexandra Lungu, Yuhuang Hu, and Michael Pfeiffer. Theory and tools for the conversion of analog to spiking convolutional neural networks. *arXiv preprint arXiv:1612.04052*, 2016.
- [37] Bodo Rueckauer, Iulia-Alexandra Lungu, Yuhuang Hu, Michael Pfeiffer, and Shih-Chii Liu. Conversion of continuous-valued deep networks to efficient event-driven networks for image classification. *Frontiers in neuroscience*, 11:682, 2017.
- [38] David E Rumelhart, Geoffrey E Hinton, and Ronald J Williams. Learning representations by back-propagating errors. *nature*, 323(6088):533–536, 1986.

- [39] Sebastian Schmitt, Johann Klähn, Guillaume Bellec, Andreas Grübl, Maurice Guettler, Andreas Hartel, Stephan Hartmann, Dan Husmann, Kai Husmann, Sebastian Jeltsch, et al. Neuromorphic hardware in the loop: Training a deep spiking network on the brainscales wafer-scale system. In *2017 international joint conference on neural networks (IJCNN)*, pages 2227–2234. IEEE, 2017.
- [40] Roy Schwartz, Jesse Dodge, Noah A Smith, and Oren Etzioni. Green ai. *Communications of the ACM*, 63(12):54–63, 2020.
- [41] Ahmed Shaban, Sai Sukruth Bezugam, and Manan Suri. An adaptive threshold neuron for recurrent spiking neural networks with nanodevice hardware implementation. *Nature Communications*, 12(1):1–11, 2021.
- [42] Sumit Bam Shrestha and Garrick Orchard. Slayer: Spike layer error reassignment in time. *arXiv preprint arXiv:1810.08646*, 2018.
- [43] David Silver, Julian Schrittwieser, Karen Simonyan, Ioannis Antonoglou, Aja Huang, Arthur Guez, Thomas Hubert, Lucas Baker, Matthew Lai, Adrian Bolton, et al. Mastering the game of go without human knowledge. *nature*, 550(7676):354–359, 2017.
- [44] Louis Sokoloff. The metabolism of the central nervous system in vivo. *Handbook of Physiology, section, I, Neurophysiology*, 3:1843–64, 1960.
- [45] Emma Strubell, Ananya Ganesh, and Andrew McCallum. Energy and policy considerations for deep learning in nlp. *arXiv preprint arXiv:1906.02243*, 2019.
- [46] Oriol Vinyals, Igor Babuschkin, Wojciech M Czarnecki, Michaël Mathieu, Andrew Dudzik, Junyoung Chung, David H Choi, Richard Powell, Timo Ewalds, Petko Georgiev, et al. Grandmaster level in starcraft ii using multi-agent reinforcement learning. *Nature*, 575(7782):350–354, 2019.
- [47] Xinxin Wang, Peng Huang, Zhen Dong, Zheng Zhou, Yuning Jiang, Runze Han, Lifeng Liu, Xiaoyan Liu, and Jinfeng Kang. A novel rram-based adaptive-threshold lif neuron circuit for high recognition accuracy. In *2018 International Symposium on VLSI Technology, Systems and Application (VLSI-TSA)*, pages 1–2. IEEE, 2018.
- [48] Jibin Wu, Yansong Chua, Malu Zhang, Guoqi Li, Haizhou Li, and Kay Chen Tan. A tandem learning rule for effective training and rapid inference of deep spiking neural networks. *IEEE Transactions on Neural Networks and Learning Systems*, 2021.
- [49] Jibin Wu, Chenglin Xu, Xiao Han, Daquan Zhou, Malu Zhang, Haizhou Li, and Kay Chen Tan. Progressive tandem learning for pattern recognition with deep spiking neural networks. *IEEE Transactions on Pattern Analysis and Machine Intelligence*, 2021.
- [50] Timo Wunderlich, Akos F Kungl, Eric Müller, Andreas Hartel, Yannik Stradmann, Syed Ahmed Aamir, Andreas Grübl, Arthur Heimbrecht, Korbinian Schreiber, David Stöckel, et al. Demonstrating advantages of neuromorphic computation: a pilot study. *Frontiers in neuroscience*, 13:260, 2019.
- [51] Han Xiao, Kashif Rasul, and Roland Vollgraf. Fashion-mnist: a novel image dataset for benchmarking machine learning algorithms. *arXiv preprint arXiv:1708.07747*, 2017.
- [52] Yexin Yan, David Kappel, Felix Neumärker, Johannes Partzsch, Bernhard Vogginger, Sebastian Höppner, Steve Furber, Wolfgang Maass, Robert Legenstein, and Christian Mayr. Efficient reward-based structural plasticity on a spinnaker 2 prototype. *IEEE transactions on biomedical circuits and systems*, 13(3):579–591, 2019.
- [53] Bojian Yin, Federico Corradi, and Sander M Bohté. Effective and efficient computation with multiple-timescale spiking recurrent neural networks. In *International Conference on Neuromorphic Systems 2020*, pages 1–8, 2020.
- [54] Friedemann Zenke, Sander M Bohté, Claudia Clopath, Iulia M Comşa, Julian Göltz, Wolfgang Maass, Timothée Masquelier, Richard Naud, Emre O Neftci, Mihai A Petrovici, et al. Visualizing a joint future of neuroscience and neuromorphic engineering. *Neuron*, 109(4):571–575, 2021.
- [55] Friedemann Zenke and Surya Ganguli. Superspike: Supervised learning in multilayer spiking neural networks. *Neural computation*, 30(6):1514–1541, 2018.
- [56] Friedemann Zenke and Tim P Vogels. The remarkable robustness of surrogate gradient learning for instilling complex function in spiking neural networks. *Neural Computation*, 33(4):899–925, 2021.

## Appendix

### A. Code availability

All code is publicly available under the BSD 3-Clause Licence on GitHub <sup>6</sup>. This includes instructions on installation, data processing and running experiments to reproduce all results and figures portrayed in the paper.

### B. Spiking neural network derivations

**Proposition 3.** Any leaky integrate and fire (LIF) model  $\tau \frac{dV(t)}{dt} = -V(t) + V_{rest} + RI(t)$  (with membrane potential  $V$ , resting potential  $V_{rest}$ , firing threshold  $V_{th}$ , resistance  $R$ , input current  $I$  and membrane time constant  $\tau$ ) can be normalised to a LIF model of the form  $\tau \frac{d\tilde{V}(t)}{dt} = -\tilde{V}(t) + \tilde{I}(t)$  (such that  $0 \leq \tilde{V}(t) \leq 1$ , with firing threshold  $\tilde{V}_{th} = 1$ , resting potential  $\tilde{V}_{rest} = 0$  and a resistance equal to one).

*Proof.* This mapping from any LIF model to the normalised LIF model is achieved using the following transformation (taken from [15]).

$$\tilde{V}(t) = \frac{V(t) - V_{rest}}{V_{th} - V_{rest}} \quad (10)$$

Rearranging this expression with respect to  $V(t) = \tilde{V}(t)(V_{th} - V_{rest}) + V_{rest}$  and substituting this into the LIF model we obtain

$$\begin{aligned} \tau \frac{dV(t)}{dt} &= -V(t) + V_{rest} + RI(t) \\ (V_{th} - V_{rest})\tau \frac{d\tilde{V}(t)}{dt} &= -\left(\tilde{V}(t)(V_{th} - V_{rest}) + V_{rest}\right) + V_{rest} + RI(t) \\ \tau \frac{d\tilde{V}(t)}{dt} &= -\tilde{V}(t) + \underbrace{\frac{R}{V_{th} - V_{rest}} I(t)}_{\text{Input current } \tilde{I}(t)} \end{aligned} \quad (11)$$

This new LIF form has a resting potential  $\tilde{V}_{rest} = 0$  and firing threshold  $\tilde{V}_{th} = 1$  (obtained by substituting  $V(t) = V_{rest}$  and  $V(t) = V_{th}$  in Equation 10 respectively). Thus, without loss of generality, any LIF model can be mapped to a normalised form using linear transformation Equation 10.  $\square$

**Proposition 4.** The normalised continuous time leaky integrate and fire model  $\tau \frac{dV(t)}{dt} = -V(t) + I(t)$  (with membrane potential  $V$ , input current  $I$  and membrane time constant  $\tau$ ) can numerically be approximated by discrete time difference equation  $V[t + 1] = \beta V[t] + (1 - \beta)I[t + 1]$ , where  $\beta = \exp(\frac{\Delta t}{\tau})$  (for simulation time resolution  $\Delta t$ ).

---

<sup>6</sup><https://github.com/webstorms/FastSNN>

*Proof.* We proceed using the forward Euler method. Let  $I(t) = I$  be constant with respect to time, for which the ordinary differential equation becomes separable.

$$\begin{aligned}
\tau \frac{dV(t)}{dt} &= -V(t) + I \\
\int \frac{dV}{V(t) - I} &= -\frac{1}{\tau} \int dt \\
\ln(V(t) - I) &= -\frac{1}{\tau} t + \ln(k) \\
V(t) &= k \exp(-\frac{1}{\tau} t) + I
\end{aligned} \tag{12}$$

For initial solution  $V(t_0)$  at time  $t_0$  we derive  $k = (V(t_0) - I) \exp(\frac{t_0}{\tau})$ . Then for constant  $I$  and initial solution  $V(t_0)$  we obtain solution.

$$\begin{aligned}
V(t) &= (V(t_0) - I) \exp(-\frac{t - t_0}{\tau}) + I \\
&= \exp(-\frac{t - t_0}{\tau}) V(t_0) + (1 - \exp(-\frac{t - t_0}{\tau})) I
\end{aligned} \tag{13}$$

To obtain the discretised update equation, we define simulation update time step  $\Delta t = t - t_0$ , decay factor  $\beta = \exp(-\frac{\Delta t}{\tau})$ , assign continuous time points to discretised time steps  $t \leftarrow t_0$  and  $t + 1 \leftarrow t_0 + \Delta t$  and assume the input current to be approximately constant and equal to  $I[t + 1]$  between discretised update steps  $t$  to  $t + 1$ .

$$V[t + 1] = \beta V[t] + (1 - \beta) I[t + 1] \tag{14}$$

□

**Proposition 5.** Equation  $V[t] = \beta^t V[0] + (1 - \beta) \sum_{i=1}^t \beta^{t-i} I[i]$  is equivalent to difference equation  $V[t] = \beta V[t - 1] + (1 - \beta) I[t]$  for  $t \geq 1$ .

*Proof.* We proceed to proof equivalence by induction. For  $t = 1$  we obtain

$$\begin{aligned}
V[1] &= \beta^1 V[0] + (1 - \beta) \sum_{i=1}^1 \beta^{1-i} I[i] \\
&= \beta^1 V[0] + (1 - \beta) I[1]
\end{aligned} \tag{15}$$

Hence the relation holds true for the base case  $t = 1$ . Assume the relation holds true for  $t = k \geq 1$ , then for  $t = k + 1$  we derive

$$\begin{aligned}
V[k + 1] &= \beta V[k] + (1 - \beta) I[k + 1] \\
&= \beta \left( \beta^k V[0] + (1 - \beta) \sum_{i=1}^k \beta^{k-i} I[i] \right) + (1 - \beta) I[k + 1] \\
&= \beta^{k+1} V[0] + (1 - \beta) \sum_{i=1}^k \beta^{(k+1)-i} I[i] + (1 - \beta) I[k + 1] \\
&= \beta^{k+1} V[0] + (1 - \beta) \sum_{i=1}^{k+1} \beta^{(k+1)-i} I[i]
\end{aligned} \tag{16}$$

This implies equivalence for  $t = k + 1$  if  $t = k$  holds true. By the principle of induction, equivalence is established given that both the base case and inductive step hold true.  $\square$

### C. Spiking speed benchmark dataset

We generated binary input spike tensors of shape  $B \times N \times T$  ( $B$  being the batch size,  $N$  the number of input neurons and  $T$  the number of simulation steps). For every batch dimension  $b$  a firing rate  $r_b \sim \mathcal{U}(u_{min}, u_{max})$  was uniformly sampled (with  $u_{min} = 0\text{Hz}$  and  $u_{max} = 200\text{Hz}$ ), from which a random binary spike matrix of shape  $N \times T$  was constructed. The spikes were generated such that every input neuron in the matrix had an expected firing rate of  $r_b\text{Hz}$ .

### D. F-MNIST dataset to spike encoding

The Fashion-MNIST is a dataset of  $28 \times 28$  images comprised of 10 different classes of fashion items (*e.g.* shoe or dress), with 60k training and 10k testing images [51]. To pass these images into the SNNs, we had to flatten each image (as we performed all experiments on feedforward non-convolutional architectures) and map every normalised image pixel value  $p$  into a spike encoding, resulting in every  $28 \times 28$  image to be transformed to new dimension  $784 \times T$  (where  $T$  is the number of simulation steps). The time of first spike was obtained using the following formula, which calculates the first spike time assuming a constant input current (which we set to be equal to the pixel value) [56] (here we set  $\tau_{eff} = 20\text{ms}$  and  $\theta = 0.2$  as done in [32]).

$$G(p) = \begin{cases} \tau_{eff} \log(\frac{p}{p-\theta}), & p > \theta \\ \infty, & \text{otherwise} \end{cases} \quad (17)$$

### E. Training details and hyperparameters

#### 4.1 Network and weight initialisation

All SNNs used in the experiments were feed-forward and fully connected, comprised of a single hidden layer and a readout layer. The readout neurons were identical to the hidden neurons, except that their firing thresholds were set to infinity (*i.e.* these neurons employed graded potentials as opposed to spikes). All synaptic weights were sampled from a uniform distribution  $\mathcal{U}(-\sqrt{\frac{1}{N}}, \sqrt{\frac{1}{N}})$  (with  $N$  being the number of input neurons to a layer) and all bias terms were initialised to 0.

#### 4.2 Supervised training loss

All networks were trained to minimise the cross-entropy loss

$$\mathcal{L} = -\frac{1}{B} \sum_{b=1}^B \sum_{c=1}^C y_{b,c} \log(p_{b,c}) \quad (18)$$

with  $B$  and  $C$  being the number of batch samples and dataset classes respectively, and  $y_{b,c} \in \{0, 1\}^C$  and  $p_{b,c}$  being the one hot target vector and network prediction probabilities respectively. The prediction probabilities  $p_{b,c}$  were obtained by passing the maximum membrane potential  $a_{b,c} = \max_t V_{b,c}^L[t]$  of every readout neuron through the softmax function.

$$p_{b,c} = \frac{\exp a_{b,c}}{\sum_{k=1}^C \exp a_{b,k}} \quad (19)$$

### 4.3 Surrogate gradient

The backprop algorithm requires all computational nodes within the computational graph of optimisation to be differentiable. This requirements is however violated in a SNN due to the non-differentiable heavy stepwise spike function  $f$ . To permit the use of backprop, we replaced the undefined derivate  $\frac{df}{dV}$  of the function  $f$  with a surrogate gradient  $\frac{df_{sur}}{dV}$  of the following form (taken from [55]), which has been shown to work well in practice [56]. Here hyperparameter  $\beta$  defines the slope of the gradient.

$$\frac{df_{sur}}{dV} = (\beta|V| + 1)^{-2} \quad (20)$$

#### 4.3.1 Training hyperparameters

	F-MNIST	N-MNIST	SHD
Number of input neurons	784	1156	700
Number of hidden neurons	200	200	200
Number of classes	10	10	20
Dataset (train/test) samples	60k/10k	60k/10k	8156/2264
Number of epochs	150	150	200
Batch size $B$	128	128	128
Simulation steps $T$	784	300	700
Time resolution $\Delta t$	1ms	1ms	2ms
Hidden neuron time constant $\tau$	10ms	10ms	10ms
Readout neuron time constant $\tau$	20ms	20ms	20ms
Surrogate gradient slope $\beta$	100	100	100
Optimiser	Adam	Adam	Adam
Learning rate	0.0002	0.0002	0.001

Table 1: Network training parameters (same parameters were used for the FastSNN and the standard SNN for every dataset).

## F. Additional speedup results



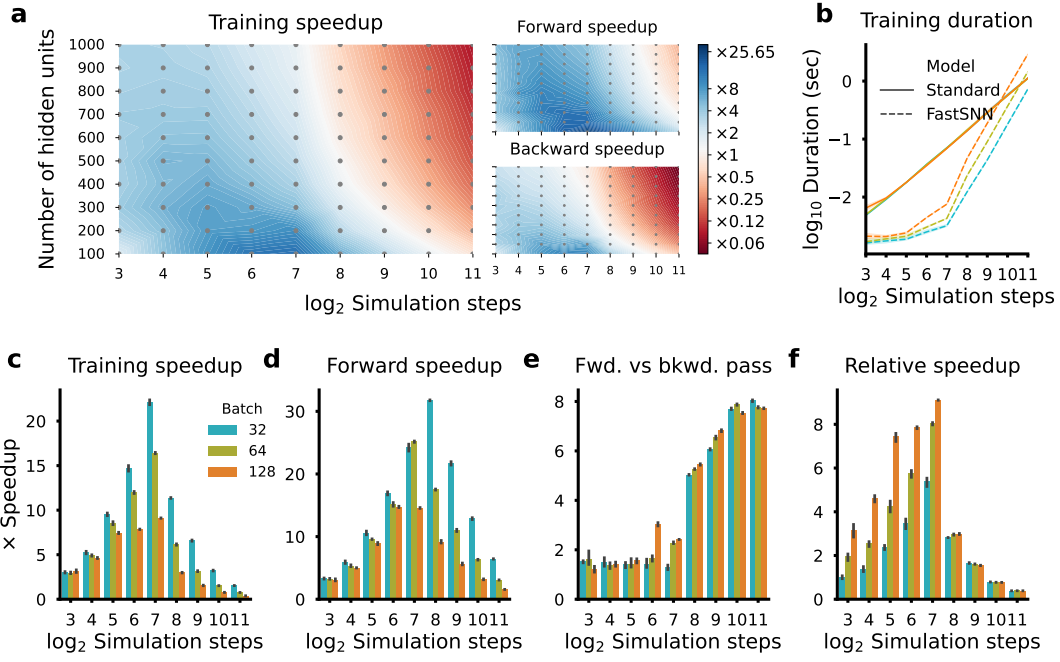


Figure 4: Speedup of the FastSNN over the standard SNN model for a single layer on a A100 GPU. **a**. Speedups as a function of the number of layer units and number of simulation steps for the total training step and the individual forward and backward passes (using a batch size  $b = 128$ ). **b**. Training durations for both models. Figures **b-f** use a layer with  $n = 200$  units and are a 10 sample average for which the mean and s.d. is plotted. **c**. Total training speedup of the FastSNN model. **d**. Forward pass speedup of the FastSN model. **e**. Forward vs the backward pass speedup of the FastSNN model. **f**. Relative speedup of the FastSNN using different batch sizes relative to the standard SNN using a fixed batch size  $b = 128$ .

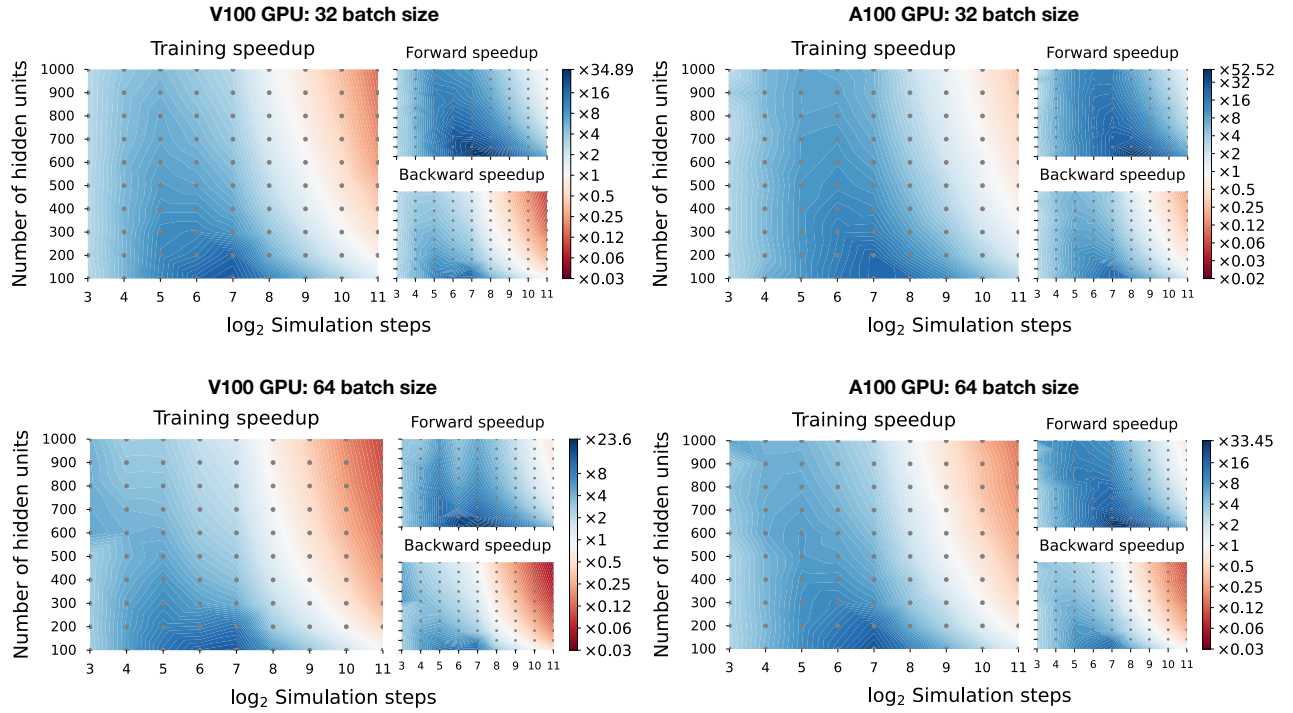


Figure 5: Speedup of the FastSNN over the standard SNN model as a function of the number of layer units and number of simulation steps for the total training step and the individual forward and backward passes. Results are portrayed for different GPUs (left: V100 and right: A100) and batch sizes (top: 32 and bottom: 64).

## Checklist

1. For all authors...
  - (a) Do the main claims made in the abstract and introduction accurately reflect the paper's contributions and scope? [\[Yes\]](#)
  - (b) Did you describe the limitations of your work? [\[Yes\]](#) See section 4.
  - (c) Did you discuss any potential negative societal impacts of your work? [\[N/A\]](#)
  - (d) Have you read the ethics review guidelines and ensured that your paper conforms to them? [\[Yes\]](#)
2. If you are including theoretical results...
  - (a) Did you state the full set of assumptions of all theoretical results? [\[Yes\]](#) See section 2.2.
  - (b) Did you include complete proofs of all theoretical results? [\[Yes\]](#) See section 2.2.
3. If you ran experiments...
  - (a) Did you include the code, data, and instructions needed to reproduce the main experimental results (either in the supplemental material or as a URL)? [\[Yes\]](#) See supplementary.
  - (b) Did you specify all the training details (e.g., data splits, hyperparameters, how they were chosen)? [\[Yes\]](#) See supplementary.
  - (c) Did you report error bars (e.g., with respect to the random seed after running experiments multiple times)? [\[Yes\]](#) All speedup benchmarks and model training was conducted multiple times.
  - (d) Did you include the total amount of compute and the type of resources used (e.g., type of GPUs, internal cluster, or cloud provider)? [\[Yes\]](#) See section 3.
4. If you are using existing assets (e.g., code, data, models) or curating/releasing new assets...
  - (a) If your work uses existing assets, did you cite the creators? [\[Yes\]](#)
  - (b) Did you mention the license of the assets? [\[Yes\]](#)
  - (c) Did you include any new assets either in the supplemental material or as a URL? [\[Yes\]](#) Datasets used to benchmark the different SNN implementations can be generated from code.
  - (d) Did you discuss whether and how consent was obtained from people whose data you're using/curating? [\[N/A\]](#)
  - (e) Did you discuss whether the data you are using/curating contains personally identifiable information or offensive content? [\[N/A\]](#)
5. If you used crowdsourcing or conducted research with human subjects...
  - (a) Did you include the full text of instructions given to participants and screenshots, if applicable? [\[N/A\]](#)
  - (b) Did you describe any potential participant risks, with links to Institutional Review Board (IRB) approvals, if applicable? [\[N/A\]](#)
  - (c) Did you include the estimated hourly wage paid to participants and the total amount spent on participant compensation? [\[N/A\]](#)